Journal of Materials Chemistry A

ROYAL SOCIETY OF CHEMISTRY

PAPER

View Article Online
View Journal

Cite this: DOI: 10.1039/d5ta04171f

Influence of highly flexible di(biphenyl)ethane units on the properties of poly(arylene piperidinium) anion exchange membranes

Si Chen,[a] Yifan Xia,[b] David Aili [b] and Patric Jannasch [*a]

Introducing angled arene units and short flexible alkyl segments into rigid aromatic heteroatom-free polymer backbones are efficient strategies to improve the performance of anion exchange membranes (AEMs). So far, only very few monomers increasing backbone flexibility in polymers prepared by polyhydroxyalkylations have been presented, often with limited reactivity and polymerizability. Here, we present the synthesis of a highly reactive monomer [*m*-di(biphenyl)ethane, *m*D] containing two angled biphenyl units bridged by an ethane link using a straightforward noble-catalyst-free reductive homocoupling reaction. A series of copolymers were produced by polyhydroxyalkylation involving *p*-terphenyl, *N*-methylpiperidone, and different concentrations of *m*D. Small angle X-ray scattering of the AEMs indicated enhanced ionic clustering with increasing *m*D content and backbone flexibility. Moreover, water and KOH (aq.) uptake, hydroxide conductivity and alkaline stability increased with the *m*D content. The hydroxide conductivity of an AEM containing 25% *m*D units reached 187 mS cm^{-1} at 80 °C in water, and an AEM with 50% *m*D units exhibited a conductivity of 53 mS cm^{-1} in 2 M KOH (aq.) solution. Using only simple nickel foam electrodes, the latter AEM reached a current density of >400 mA cm^{-2} at 2.5 V without any cell optimization. In summary, this work demonstrates a convenient synthetic strategy to incorporate flexible units in rigid aromatic polymers, offering improved membrane properties and valuable insights into the design and optimization of advanced AEM materials.

Received 23rd May 2025
Accepted 19th August 2025

DOI: 10.1039/d5ta04171f

rsc.li/materials-a

1. Introduction

Meeting current climate and sustainable energy challenges requires the innovation and development of novel clean energy devices.[1] In this context, anion exchange membrane fuel cells (AEMFCs) and anion exchange membrane water electrolyzers (AEMWEs), operating under alkaline conditions, are of significant interest in the pursuit of low-cost clean energy because of the potential for noble-metal-free catalysts and electrodes.[2,3] Anion exchange membranes (AEMs) are crucial components in these electrochemical devices, separating the electrodes and facilitating the transport of water and hydroxide ions between the electrodes.[4,5] In addition, AEMs are utilized in redox flow batteries and CO_2 electrolyzers.[4]

Initially, AEMs based on aryl ether polymers, including poly(phenylene oxide)s, poly(arylene ether sulfone)s, and poly(arylene ether ether ketone)s, were investigated.[6–8] These polymers are comparatively inexpensive, and the flexible ether bonds between the rigid phenyl rings enhance the mechanical properties of the AEMs by reducing brittleness.[6] However, the ether bonds were later proven to cause polymer chain degradation under harsh alkaline conditions.[4,9] To meet the demands of high alkaline stability and ion conductivity, aryl ether-free poly(arylene alkylene)s synthesized *via* superacid-mediated polyhydroxyalkylation reactions are currently extensively studied for use as AEMs.[10–21] Polyhydroxyalkylation reactions require electron-rich arene monomers, such as terphenyls and fluorenes, and suitable ketone or aldehyde monomers and offer many possibilities to vary the polymer structure and functionality. Under optimized conditions, polyhydroxyalkylations generate high-molecular weight poly(arylene alkylene)s while tolerating various functional groups.[10,11] Hence, this type of polymerization provides a robust and versatile platform for developing high-performance AEMs.[4,10–14] However, the ether-free poly(arylene alkylene) backbones produced by polyhydroxyalkylation often lack the proper mechanical toughness, particularly when containing rigid *p*-terphenyl or dimethyl fluorene units. This adversely affects the film-forming and mechanical properties, as well as the stability of AEMs.[17,18]

A feasible method to increase the backbone flexibility of poly(arylene alkylene)s is to copolymerize with an angled arene monomer like *m*-terphenyl, having a torsion angle between two adjacent benzene rings (Scheme 1a). This approach leads to much more flexible polymers compared to when the non-angled *p*-terphenyl monomer is used.[13,16] Bae *et al.* demonstrated that

[a]*Department of Chemistry, Lund University, P. O. Box 124, SE-22100 Lund, Sweden*
[b]*Department of Energy Conversion and Storage, Technical University of Denmark, Elektrovej, Building 375, Lyngby, 2800, Denmark. E-mail: patric.jannasch@chem.lu.se*

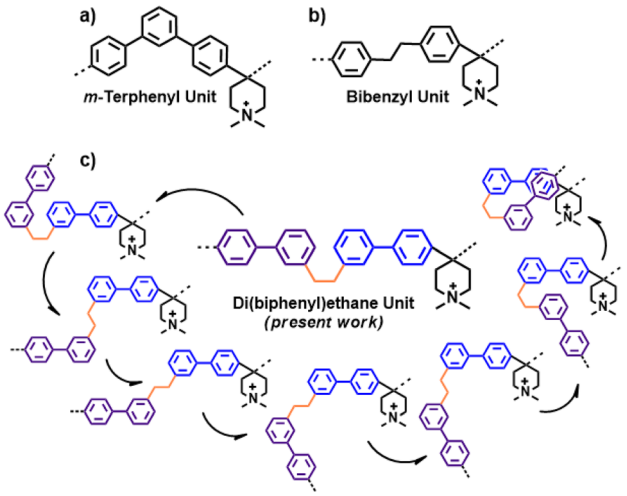

Scheme 1 Poly(arylene piperidinium) segments containing (a) an angled arene unit (*m*-terphenyl[22]), (b) a short flexible alkyl bridge (bibenzyl[25]), and (c) the di(biphenyl)ethane unit studied in the present work. The latter unit combines the features of *m*-terphenyl and bibenzyl units, and introduces exceptional polymer chain flexibility.

poly(*m*-terphenylene alkylene)s with pendant quaternary ammonium groups can be applied in AEMFCs to achieve a higher power density compared to the corresponding devices using poly(*p*-terphenylene alkylene)-based AEMs.[13] Under similar preparation conditions, the poly(*m*-terphenylene alkylene)s also reached a higher molecular weight than their *p*-terphenyl-based isomer. This may originate from the higher solubility of poly(*m*-terphenylene) during the polyhydroxyalkylation process. Further research has shown that optimization of the *m*-terphenyl-to-*p*-terphenyl ratio in poly(terphenyl piperidinium) AEMs can improve stability, conductivity, and the performance of the AEMs.[13,22–24]

Recently, Lee *et al.* used bibenzyl, consisting of two benzene rings bridged by an ethyl group, to introduce backbone flexibility in poly(arylene piperidinium)s (Scheme 1b), thus enabling excellent AEMFC performance, including a peak power density of 2.58 W cm^{-2}.[25] They later investigated the effect of the alkyl chain length in-between the benzene rings on the physical and electrochemical performance of the AEMs.[26]

Currently, the range of available flexible arene monomers for polyhydroxyalkylation is limited. In addition, arene monomers with bridging alkyl segments often exhibit low reactivity in polyhydroxyalkylation polymerizations.[25–27] Consequently, there is a need for novel, reactive, and flexible arene monomers for the preparation of high-performance AEMs. Combining the characteristics of the aforementioned *m*-terphenyl and bibenzyl monomers presents a promising strategy for developing new monomers to increase backbone flexibility.[27–29] In this context, we have in the present work designed and synthesized a novel monomer [*m*-di(biphenyl)ethane (*m*D)] for use in polyhydroxyalkylations, incorporating both angled arene units and alkyl segments (Scheme 1c). Monomer *m*D was prepared *via* a noble-metal-free reductive coupling reaction in an almost quantitative conversion. To investigate the influence of the *m*D units on AEM properties, we have synthesized a series of poly(arylene piperidinium)s with different *m*D : *p*-terphenyl ratios to vary the backbone flexibility. AEMs were then prepared *via* solution-casting and characterized with respect to morphology, water/alkaline uptake, mechanical properties, ionic conductivity, and alkaline and thermal stability. Subsequently, the most promising AEM was selected for an initial water electrolysis evaluation, as well as tensile testing, to investigate the use of these AEMs in electrochemical energy devices.

2. Experimental section

Information on the materials used and details concerning the measurements performed are included as SI.

2.1. Monomer synthesis

The *m*D monomer was synthesized following a published procedure after slight modification.[30,31] Anhydrous cobalt chloride (26 mg, 0.2 mmol, 2 mol%) was added to a 50 mL Schlenk tube equipped with an oval magnetic stirring bar. The Schlenk tube was sealed with a rubber septum, evacuated, and backfilled with nitrogen thrice. Subsequently, 15 mL of anhydrous THF was injected before adding 0.8 mL 1 M trimethyl phosphine (0.8 mmol, THF solution). After the addition of 6 mL 1 M dimethyl zinc (6 mmol, heptane solution), the black solution in the Schlenk tube became clear and dark red. An amount of 2.47 g (10 mmol) 3-phenyl benzyl bromide was dissolved in 5 mL THF before being quickly added to the Schlenk tube. The tube was immediately placed in a sand bath preheated to 66 °C. The reaction was stopped after 20 min. by adding 1 mL 2 M HCl (aq.) solution. Next, the reaction mixture was dissolved in 200 mL dichloromethane (DCM) and washed with water thrice. The organic phase was collected and filtered through a pad of aluminum oxide until the solution became colorless. The resulting solution was dried with Na_2SO_4, and the organic solvent was removed using a rotary evaporator. A clear, highly viscous liquid was obtained, which spontaneously crystallized within 10 min. After drying under vacuum at room temperature for 2 h, 1.64 g (4.9 mmol) *m*D monomer (quantitative conversion) was ready for polymerization. ^{1}H NMR (400 MHz, chloroform-*d*) δ 7.66 (dd, J = 8.3, 1.3 Hz, 4H), 7.56–7.38 (m, 12H), 7.29 (dt, J = 7.5, 1.5 Hz, 2H), 3.13 (s, 4H). ^{13}C NMR (101 MHz, chloroform-*d*) δ 142.24, 141.41, 128.88, 128.78, 127.58, 127.53, 127.28, 124.97, 38.15.

2.2. Polymerization and quaternization

A series of precursor copolymers were synthesized *via* superacid-mediated polyhydroxyalkylations of *m*D, *p*-terphenyl, and *N*-methyl piperidone.[11] The copolymers were designated as P*m*DPip-*x*, where *x* is the mol% of *m*D units. Here, the synthesis of P*m*DPip-100 is given as an example. To a 25 mL round-bottom flask equipped with a magnetic stirrer, *m*D (334 mg, 1 mmol) and *N*-methyl piperidone (147 mg, 1.3 mmol) were added along with 1.2 mL DCM. The mixture was cooled to 0 °C in an ice bath before adding 0.2 mL trifluoroacetic acid (TFA).

Trifluoromethansulfonic acid (TFSA, 1.4 mL, 15.6 mmol) was then added dropwise. The polymerization was allowed to proceed at room temperature for 4 h, after which 10 mL of dimethyl sulfoxide (DMSO) was added to dilute the viscous solution. The solution was then poured into 100 mL of a 1 : 1 (v : v) mixture of diethyl ether and isopropanol to precipitate the product as a white powder. The product was collected and dried in a vacuum oven at 50 °C, yielding P*m*DPip-100 quantitatively (447 mg).

Quaternization of the precursor polymers was achieved in Menshutkin reactions with methyl iodide.[16] The samples were designated as P*m*DPipQ-*x*, and here the synthesis of P*m*DPipQ-100 is provided as an example. To a 25 mL round-bottom flask equipped with a magnetic stirrer, P*m*DPip-100 (430 mg, corresponding to 1 mmol *N*-methylpiperidine units), K_2CO_3 (280 mg, 2 mmol), and methyl iodide (0.17 mL, 2.5 mmol, 5 equiv.) were added together with 10 mL DMSO. The flask was sealed and covered with aluminum foil. After stirring for 24 h, the solution was poured into water to precipitate the product, yielding P*m*DPipQ-100 as a white solid. The product was washed with a mixture of isopropanol and diethyl ether, then collected and dried under vacuum. P*m*DPipQ-100 was obtained quantitatively (576 mg).

2.3. Membrane casting

An amount of 200 mg of each P*m*DPipQ-*x* sample was first dissolved and diluted with dimethyl sulfoxide (DMSO) to reach a concentration of 4 wt% polymer. The solutions were passed through a PTFE filter (ϕ = 5 μm), before being poured into a Petri dish (ϕ = 6 cm). Casting was performed during 2 days at 80 °C in an air-circulating oven, after which transparent, colorless, and uniform AEMs were obtained. The AEMs were subsequently immersed in 1 M aq. NaBr for 2 days, before washing and storage in deionized water (DI water).

3. Results and discussion

3.1. Synthesis of monomers and polymers

One of the major motivations for developing devices based on AEMs is their potential to utilize non-noble metals as catalysts and electrodes. Hence, it is also important to avoid the use of noble metal-catalyzed reactions in the preparation of the AEMs. Unlike conventional methods to prepare arene-functionalized monomers that often require Pd-catalyzed Suzuki-cross-coupling reactions involving both aryl boronic acids and aryl halides,[32–34] the symmetrical *m*D monomer was synthesized in a cobalt-catalyzed reductive homocoupling reaction of only one benzyl bromide compound.[30,31,35] In this coupling reaction, a low-valent cobalt species abstracts the bromine atoms from the starting benzyl bromide compound, and then the combination of the generated benzylic radicals efficiently forms the C_{sp^3}–C_{sp^3} bond of *m*D (Scheme 2a). The cobalt(II) species was then regenerated to cobalt(0) using dimethyl zinc.[36] The monomer was quantitatively isolated by crystallization without needing column chromatography (Fig. 1a and b). This straightforward synthetic method indicates possibilities for scaled-up production of *m*D. In addition, manganese has recently been identified as a potential alternative to dimethyl zinc, which may further reduce the cost of *m*D.[37]

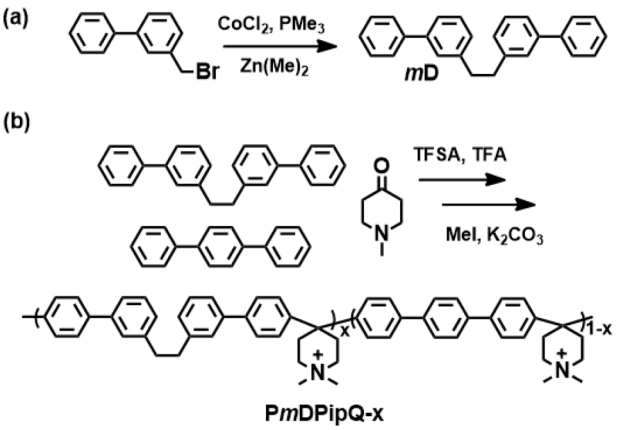

Scheme 2 (a) Synthesis of the *m*D monomer and (b) the preparation of the P*m*DPipQ-*x* series of AEM polymers by superacid-mediated polyhydroxyalkylations (*x* indicating the mol% of *m*D units).

The *m*D monomer obtained in the crystalline form was then employed in superacid-mediated polyhydroxyalkylations with *N*-methylpiperidone and *p*-terphenyl (Scheme 2b). Quaternization of the *N*-methyl piperidine groups in the polymer backbones was subsequently achieved by Menshutkin reactions with methyl iodide, yielding the P*m*DPipQ-*x* series of polymers (*x* indicating the mol% of *m*D units in the polymer). Compared to bibenzyl-type monomers, *m*D exhibited a significantly higher reactivity. This enabled a high-molecular weight polymer based on only *m*D and *N*-methyl piperidone (P*m*DPipQ-100) to be formed after merely 4 h. Additionally, when copolymerized with *p*-terphenyl, the resulting ratios between the *p*-terphenyl and *m*D units (calculated from NMR data) precisely matched the monomer feed ratios (Table S1). Similar to *m*-terphenyl, the presence of the *m*D units enhanced polymer solubility during the polymerization reaction, which may explain why P*m*DPipQ-25 (with the lowest *m*D content) displayed a relatively low intrinsic viscosity (Table 1).

3.2. Membrane preparation and morphology

All the AEMs cast from DMSO solutions were transparent, mechanically robust, and foldable (180°). After casting, the membranes were ion-exchanged to the Br^- form and the ion exchange capacity (IEC) was determined by Mohr titrations. The results aligned well with the theoretical IEC values calculated from the corresponding polymer structures (Table 1). As the content of *m*D units increased from 25 to 100%, the IEC of the AEMs decreased from 2.59 to 2.16 mequiv. g^{-1}. Reduced ionic content often leads to membrane morphologies with less organized phase domains, observed by indistinct ionomer peaks in the small angle X-ray scattering (SAXS) profiles.[38] However, despite having the lowest IEC, P*m*DPipQ-100 showed the strongest ionomer peak, stronger than the ionomer peaks of all the copolymers containing *p*-terphenyl (Fig. 2a). Notably, the

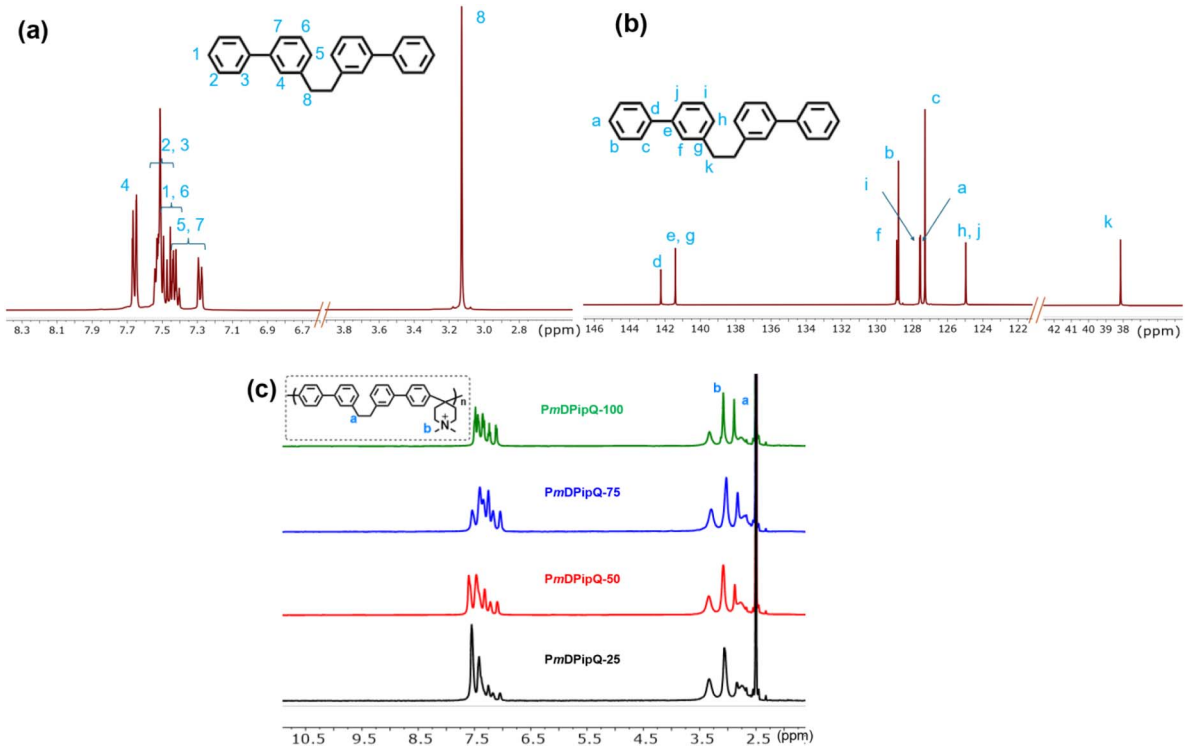

Fig. 1 (a) ^{1}H and (b) ^{13}C NMR spectra of the *m*D monomer recorded in chloroform-*d*, and (c) ^{1}H NMR spectra of the samples in the P*m*DPipQ-*x* series recorded in DMSO-d_6 solutions (TFA was added to shift the water signal).

intensity of the ionomer peak gradually increased with the *m*D unit content of the membranes (corresponding to a decreasing IEC), which indicated that the increasing polymer chain flexibility favored the ionic clustering more than the increasing ionic content. In comparison, ionomer peaks are not normally observed for AEMs based on poly(*p*-terphenyl piperidinium), indicating less ordered and inefficient ionic clustering and phase separation of more stiff polymer backbones.[14,16]

While SAXS data provide information about the bulk morphology, atomic force microscopy (AFM) analysis gives details about surface morphology. As seen in Fig. 2b–e, AFM phase images also indicated distinctly phase separated morphologies for all the AEMs, with bright and dark areas indicating hydrophobic and hydrophilic phase domains, respectively. As the *m*D content of the membranes increased, the regularity of the phase domains increased, which aligned with the SAXS results. Concurrently, the overall area of hydrophobic phase domains increased with the *m*D content, which was consistent with decreasing IEC values.

3.3. Thermal properties

Previous studies have demonstrated that the chemical (alkaline) stability of the piperidinium cation is significantly improved by placement on flexible segments in the backbone to allow ring relaxation.[19,23] Moreover, the incorporation of monomer units containing flexible alkyl chains in the backbone has been reported to improve the thermal stability of piperidinium-functional AEMs.[26,27] In the present case, the thermal decomposition and stability of the AEM samples in the Br^- form were studied by thermogravimetric analysis (TGA) under nitrogen and air atmosphere (Fig. S7a and b, respectively), to measure the thermal decomposition temperature ($T_{d,95}$, taken at 5%

Table 1 Key AEM properties

AEM	IEC (mequiv. g^{-1})		WU^a (%) (80 °C)	λ^a (80 °C)	2 M aq. KOH uptake (%, 80 °C)	σ^a (mS cm^{-1})		T_g (°C)	$T_{d,95}$ (°C)	[η], dL g^{-1}
	Theoretical	Titrated				Water^a	2 M KOH			
P*m*DPipQ-25	2.59	2.59	197	42	112	187	33	—	313	0.73
P*m*DPipQ-50	2.43	2.47	502	113	151	253	53	210	420	0.81
P*m*DPipQ-75	2.29	2.32	769	184	171	338	42	175	423	0.82
P*m*DPipQ-100	2.16	2.21	—	—	174	—	43	159	424	0.86

^{a} Measured in the OH^- form.

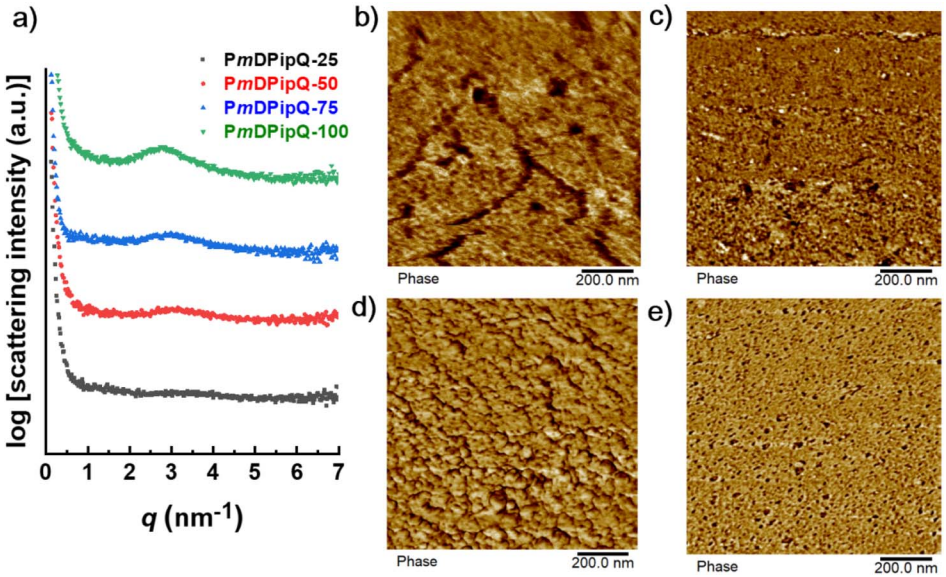

Fig. 2 (a) SAXS profiles of dry AEMs in the Br^- form, and AFM phase images of dry AEMs: (b) P*m*DPipQ-25, (c) P*m*DPipQ-50, (d) P*m*DPipQ-75, and (e) P*m*DPipQ-100 in the Br^- form.

weight loss). Membrane PTPipQ-1 (with only *p*-terphenyl units) has been reported to reach $T_{d,95}$ = 264 °C under nitrogen.[14] The incorporation of 25% flexible *m*D units raised the $T_{d,95}$ value of P*m*DPipQ-25 to 313 °C (Table 1). Increasing the content of flexible *m*D units to 50% resulted in an additional increase of $T_{d,95}$ to 420 °C for P*m*DPipQ-50. Further increases in the *m*D content, beyond 50%, did not lead to any significant increases in $T_{d,95}$, and P*m*DPipQ-75 and P*m*DPipQ-100 reached $T_{d,95}$ values of 423 and 424 °C, respectively. Based on this finding, we speculate that enhancing backbone flexibility raises the thermal stability of the piperidinium cation. However, this positive effect levels out after reaching a certain critical backbone flexibility.

As expected, the TGA thermograms recorded under air showed lower $T_{d,95}$ values compared to those under nitrogen (Fig. S7b). The thermo-oxidative decomposition revealed a multi-step process, with the first two steps most probably related to the degradation of the piperidinium cations. Also in this case, the $T_{d,95}$ values increased with the *m*D content, and P*m*DPipQ-25, -50, -75, and -100 showed values of 276, 302, 387, and 411 °C, respectively.

The AEMs were characterized by differential scanning calorimetry (DSC, Fig. S7c), and glass transitions were observed at T_g = 210, 175, 159 °C for P*m*DPipQ-50, P*m*DPipQ-75, and P*m*DPipQ-100, respectively. Hence, as expected, the T_gs of the AEMs decreased, and the specific heat capacity (ΔC_p) increased, with the *m*D content. These features indicated increasing backbone flexibility with the *m*D content. Moreover, P*m*DPipQ-50, P*m*DPipQ-75, and P*m*DPipQ-100 had T_gs below their respective $T_{d,95}$ values, suggesting that these samples were in the rubbery-melt state when thermally decomposing in the TGA experiments. Hence, the high backbone flexibility under these conditions may have efficiently prevented the distortion of piperidinium rings, which may in turn explain the observed increase in the thermal stability. In contrast, no T_g was detected for P*m*DPipQ-25 below its degradation temperature, which may explain why the $T_{d,95}$ for this AEM was the lowest among all four samples.

3.4. Aqueous uptake and swelling

For application in AEMFCs, AEMs with a suitable level of water uptake are a prerequisite for efficient ion conduction and water management.[39] The water uptake typically depends on, *e.g.*, the IEC value, polymer backbone flexibility, degree of crystallinity, and the molecular weight. In the present case, the water uptake and swelling ratio of the AEMs in the P*m*DPipQ-*x* series (OH^- form) were measured between 20 and 80 °C, and the results are shown in Fig. 3a, c, and e, respectively. On the one hand, AEMs with a high *m*D content have lower IEC values compared to those with a high *p*-terphenyl content, which should result in a reduced water uptake with increasing *m*D content. On the other hand, an increased *m*D content can be expected to significantly increase the polymer backbone flexibility of the polymers, which promotes water uptake. Although these two parameters linked to the *m*D content have opposing effects, the overall impact of the increased backbone flexibility provided by the *m*D units dominated. Hence, the water uptake of the P*m*DPipQ-*x* membranes increased with the *m*D content. Membrane P*m*DPipQ-25, with the lowest *m*D content, exhibited the lowest water uptake (197% at 80 °C) in this work. Correspondingly, P*m*DPipQ-50 and P*m*DPipQ-75 showed a higher water uptake, and the water uptake started to increase progressively with temperature above 60 °C. P*m*DPipQ-75 softened considerably when the water uptake reached 769%, corresponding to a hydration number (λ) of 184, at 80 °C. Consequently, the OH^- concentration of the swollen P*m*DPipQ-75 decreased to approximately 1.2 mol L^{-1}. For P*m*DPipQ-100, the progressive increase in water uptake started already at 40

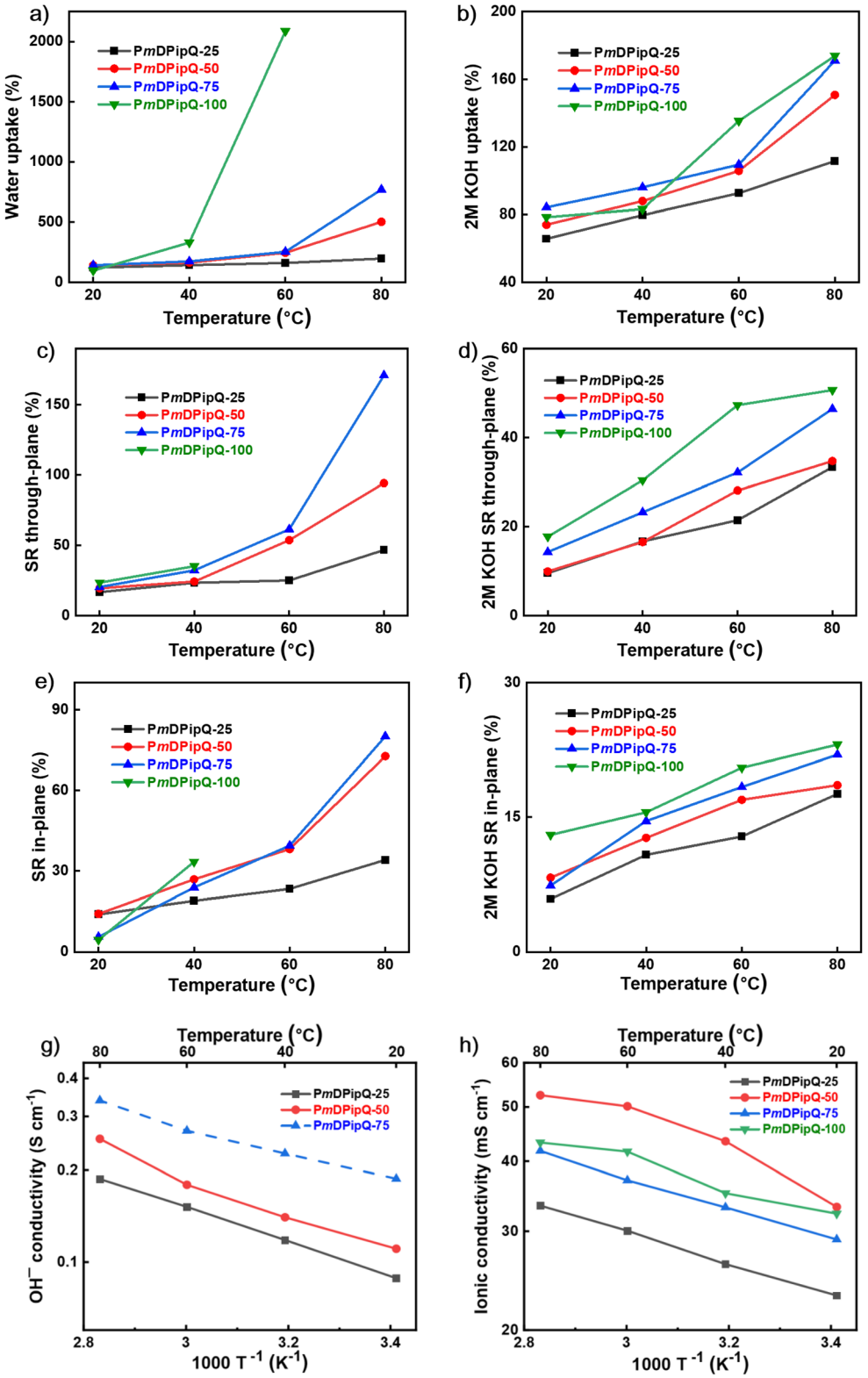

Fig. 3 Water uptake, swelling and ionic conductivity data of the AEMs in the P*m*DPipQ-*x* series between 20 and 80 °C (note different scales on vertical axes): water uptake (a) and uptake of 2 M aq. KOH (b), through-plane swelling ratio in water (c) and in 2 M aq. KOH (d), in-plane swelling ratio in water (e) and in 2 M aq. KOH (f), OH^- conductivity in the fully hydrated state [immersed in water] (g) and ionic conductivity in 2 M aq. KOH solution (h).

°C, in agreement with the lower T_g observed by DSC. This membrane became a hydrogel and lost all mechanical strength after 8 h immersion in water at 80 °C. The swelling ratio of the AEMs followed the same trend as the water uptake (Fig. 3c and e), with P*m*DPipQ-25 and P*m*DPipQ-50 showing controlled swelling ratios at 80 °C.

In practical applications, AEMWEs generally operate with electrolyte solutions rather than pure water.[40] Since the uptake of alkaline solution of AEMs is often significantly lower than the uptake of water, it is relevant to evaluate the alkaline solution uptake of the P*m*DPipQ-*x* AEMs. Hence, the electrolyte uptake and swelling ratio were measured in 2 M aq. KOH between 20 and 80 °C (Fig. 3b, d and e). As expected, the electrolyte uptake and swelling ratio of the AEMs increased with both temperature and *m*D content. In contrast to the water uptake data, the difference in electrolyte uptake between the AEMs was modest. P*m*DPipQ-100 exhibited the highest alkaline solution uptake, reaching 174% at 80 °C. All AEMs remained mechanically robust after the alkaline solution uptake, also at 80 °C.

3.5. Ionic conductivity

The in-plane OH^- conductivity of the AEMs fully immersed in water was measured between 20 and 80 °C using electrochemical impedance spectroscopy (EIS). In addition, the through-plane ionic conductivity of the AEMs immersed in 2 M aq. KOH solution was measured between 20 and 80 °C, using a previously reported method.[41] The OH^- conductivity is an essential property of AEMs and depends on various factors, such as water/electrolyte uptake, temperature, and membrane morphology. As described above, increasing amounts of *m*D in the P*m*DPipQ-*x* series reduced the IEC values, but increased the uptake of water and 2 M aq. KOH solution at 80 °C. As seen in Fig. 3g, the OH^- conductivity of the P*m*DPipQ-*x* membranes in the fully hydrated state generally increased with decreasing IEC and increasing water uptake. Compared to poly(*p*-terphenyl piperidinium) [PTPipQ100, with only *p*-terphenyl in the backbone, 132 mS cm^{-1}, 302% water uptake at 80 °C],[14,16] P*m*DPipQ-25 exhibited higher conductivity (184 mS cm^{-1}) at a lower water uptake. P*m*DPipQ-50 and P*m*DPipQ-75 reached very high OH^- conductivities, *i.e.*, 253 mS cm^{-1} and 338 mS cm^{-1} at 80 °C, respectively. These levels of conductivities have only rarely been reported previously. However, a gel-state ion-solvating polybenzimidazole membrane doped with 25 wt% KOH has recently been reported by Henkensmeier *et al.* to reach 313 mS cm^{-1} at 80 °C.[47] Furthermore, a highly swollen ion-solvating membrane based on a sulfonated polybenzimidazole has been reported by the same authors to reach an even higher conductivity, 358 mS cm^{-1} when doped with 1 M KOH at 80 °C.[48] This value further increased to 682 mS cm^{-1} with 3 M KOH. As mentioned above, the water uptake of P*m*DPipQ-75 increased to 769% at 80 °C, which transformed the membrane to a self-supporting gel-like material with an OH^- concentration close to 1.2 M. Furthermore, the dimensional increase during the conductivity measurements between 20 and 80 °C may have led to a certain overestimation of the OH^- conductivity of this membrane, since the standard OH^- conductivity calculation was based on the dimensions of the membrane equilibrated at room temperature. It should be mentioned that the P*m*DPipQ-75 sample swelled significantly in the EIS cell during the temperature increase from 20 to 80 °C. This dimensional change may have led to an overestimation of the OH^- conductivity of this membrane, since the standard calculation of the OH^- conductivity was based on the initial thickness of the membrane equilibrated at room temperature. The OH^- conductivity of P*m*DPipQ-100 was not reported because of the very high water uptake at 80 °C. The uptake decreased significantly when the AEMs were immersed in aq. KOH solution. Moreover, the backbone flexibility appeared to have a significantly lower effect on the ionic conductivity in 2 M aq. KOH solution, and the ionic conductivity did not increase with the *m*D content. P*m*DPipQ-50 had a moderate alkaline solution uptake and reached the highest conductivity among the AEMs, just above 50 mS cm^{-1} at 80 °C, while P*m*DPipQ-25 with the lowest alkaline solution uptake among the AEMs reached the lowest OH^- conductivity at 80 °C, *i.e.*, 33 mS cm^{-1}.

3.6. Alkaline stability

Reaching a sufficient alkaline stability of the AEMs is a major challenge for application in AEMFCs and AEMWEs. Previous research has demonstrated that the alkaline stability of the *N*,*N*-dimethyl piperidinium cation can be significantly improved by reducing the constraints of the piperidine ring in the polymer structure, either by increasing backbone flexibility or by tethering the cations to the polymer backbone *via* flexible side chains.[3]

Consequently, the alkaline stability of the P*m*DPipQ-*x* was expected to increase with the *m*D content. However, after storage in 5 M aq. KOH at 80 °C for 480 h, all the AEMs exhibited approximately 6% total ionic loss despite different contents of the flexible *m*D units (Fig. 4). Hofmann elimination was identified as the dominating degradation reaction leading to ionic loss, as indicated by the small signals at 4.9, 5.3, 6.5, (b, c, d in Fig. 4) arising from the vinyl group in the degradation product, and at 9.7 ppm (a in Fig. 4) originating from the protonated tertiary amine group in the degradation product. As expected, the ratios of these signals were 1 : 1 : 1 : 1.

The present AEMs showed slightly higher alkaline stability compared to the corresponding poly(arylene piperidinium) AEMs based on terphenyl and quaterphenyl,[14,34] which may result from the higher backbone flexibility induced by the *m*D units. However, the content of flexible *m*D units appeared to have little influence on the alkaline stability of the P*m*DPipQ-*x* AEMs. The reason may be that the flexible units had a limited effect on the local chain rigidity around the piperidinium rings along the polymer backbone. Despite different *m*D contents, the piperidinium rings are still surrounded by rigid biphenyl and *p*-terphenyl units that may distort the rings (Scheme 2b). Moreover, all the P*m*DPipQ-*x* AEMs had almost the same uptake of KOH solution (Fig. 3b), which may also have contributed to a similar alkaline stability. The alkaline stability of quaternary ammonium cations generally increases with the λ (hydration number, $[H_2O]/[OH^-]$).[42] Since the uptake of pure water

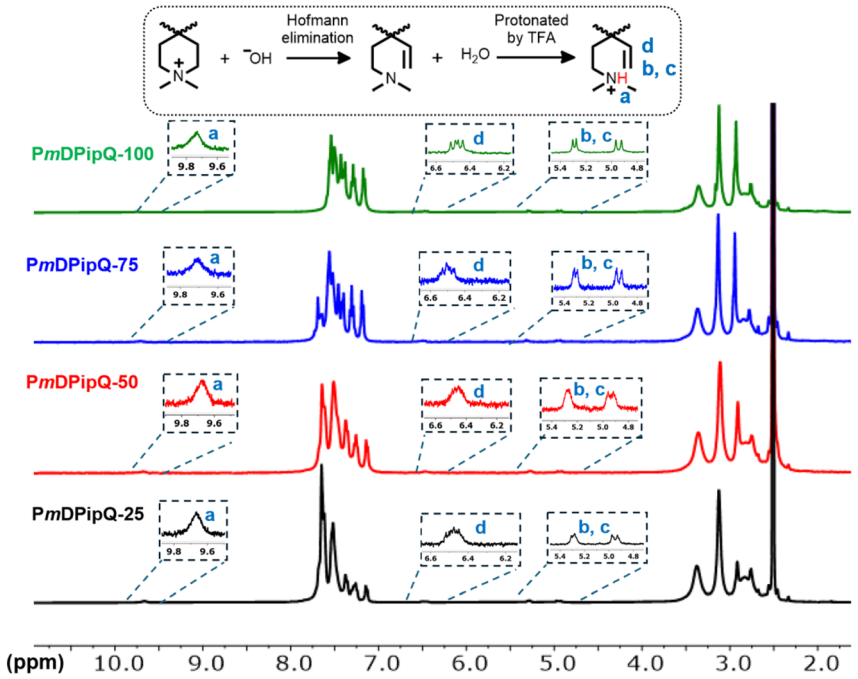

Fig. 4 ^{1}H NMR spectra of AEM samples after storage in 5 M aq. KOH solutions at 80 °C for 480 h, displaying small signals (a–d) emerging from the degradation products by Hofmann β-elimination.

increased with the *m*D content, the alkaline stability of the AEMs in pure water can be expected to increase with the *m*D content.

3.7. Tensile testing

Good mechanical properties of AEMs are required to prevent rupture and provide support for the electrochemical cell structure. Some of the P*m*DPipQ-*x* membranes showed high alkaline stability and OH^- conductivity in 2 M KOH (aq.) solution, and the mechanical properties of the AEMs were characterized to further assess the suitability for water electrolyzer applications. The stress–strain data of the AEMs recorded in the dry state and after immersion in 2 M KOH (aq.) solution are presented in Fig. 5a and b, respectively. As the *m*D content increased from 25 to 75%, both the tensile strength and the elongation at break increased. In the dry state, the P*m*DPipQ-50 and P*m*DPipQ-75 demonstrated a tensile strength over 75 MPa with an elongation at break exceeding 30%. These values surpass the corresponding data of membranes where polymer backbone flexibility was introduced solely through twisted arene moieties[34] or short alkyl chains.[26] P*m*DPipQ-100, without any *p*-terphenyl units, exhibited a lower elongation at break compared to P*m*DPipQ-50 and P*m*DPipQ-75, and showed the lowest tensile strength among the AEMs. Seemingly, the mechanical properties of the former sample deteriorated because of the very high *m*D content, which made the AEM very soft and weak. The findings agree with the previous findings that an appropriate polymer backbone flexibility may enhance the mechanical properties of AEMs by reducing brittle behavior.[22] Since AEMs often operate immersed in KOH solutions, the stress–strain curves of the AEMs in 2 M KOH (aq.) were also measured (Fig. 5b). As expected, under this condition, the AEMs became considerably softer than in the dry state, resulting in decreased tensile strength and increased elongation at break. P*m*DPipQ-50 and P*m*DPipQ-75 exhibited a tensile strength over 20 MPa and an elongation at break exceeding 70%, making them promising candidates for use in alkaline electrochemical devices.

3.8. Initial water electrolysis testing

Displaying high alkaline stability and OH^- conductivity, as well as good mechanical properties, the P*m*DPipQ-50 membrane was selected for a preliminary evaluation in a water electrolyzer to investigate the applicability of AEMs based on poly(arylene piperidinium)s containing *m*D units in electrochemical devices. The single cell assembly followed a previously reported method.[43,44] A 60 μm thick P*m*DPipQ-50 membrane was sandwiched between a pair of pure nickel foam sheets as electrodes in the cell hardware. The test was conducted with 2 M KOH (aq.) at 40, 60 and 80 °C, respectively. The polarization curves are displayed in Fig. 6a, with the corresponding galvanostatic electrochemical impedance spectroscopy (GEIS) results presented in Fig. 6b. An inset image in Fig. 6b compares the potentiostatic electrochemical impedance spectroscopy (PEIS) and GEIS data at 80 °C. The *in situ* conductivities estimated from PEIS data recorded at 1.3 V (without any gas evolution), and from GEIS data recorded at 10 mA cm^{-2} and 100 mA cm^{-2} (with increasing gas evolution), were 12, 8, and 6 mS cm^{-1}, respectively. The difference between the conductivities estimated from the PEIS and GEIS data may be attributed to the entrapment of H_2 gas in the nickel foam, causing additional

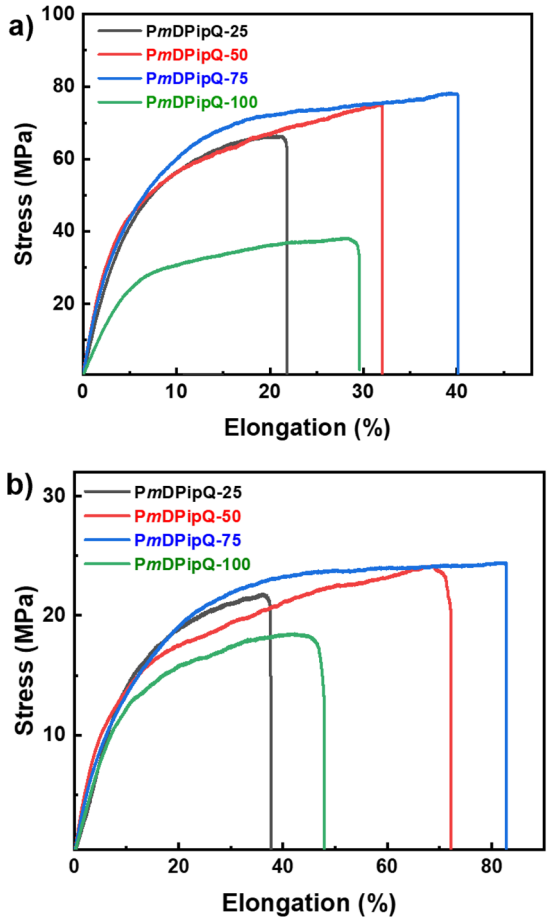

Fig. 5 Stress–strain data of AEMs in the dry state (a) and after immersion in 2 M KOH (aq.) solution (b).

resistance contributions from the porous electrodes. These *in situ* conductivities were significantly lower than the *ex situ* conductivity results, which may indicate additional resistance contributions from the electrolyzer cell fixture, including contact resistance between the electrode and the flow fields. For this reason, the current density only reached 400 mA cm^{-2} at 2.5 V and 80 °C (Fig. 6a). Consequently, more advanced electrodes and catalysts that better match the flexible membrane are required to increase the AEMWE performance.

The lower explosion limit of H_2/O_2 mixtures is merely 3.8 mol% at 80 °C,[45] and the H_2 crossover is therefore a critical factor when evaluating the safety of AEMWEs. Transport mechanisms, including diffusion and convection of H_2-supersaturated electrolyte from the cathode into the anode compartment, contribute to the overall permeation of H_2 through the membrane.[46] The H_2/O_2 level in the cell assembled with P*m*DPipQ-50 is shown in Fig. 6c. At 80 °C, the H_2/O_2 level remained below 0.7% at 50 mA cm^{-2} and decreased to 0.4% at 100 mA cm^{-2}, thus ensuring safe operation of AEMWEs assembled with this AEM. In addition, the cell voltage (Figure S8) required to achieve 50 mA at 40 °C before and after the H_2 crossover measurement, which was performed during

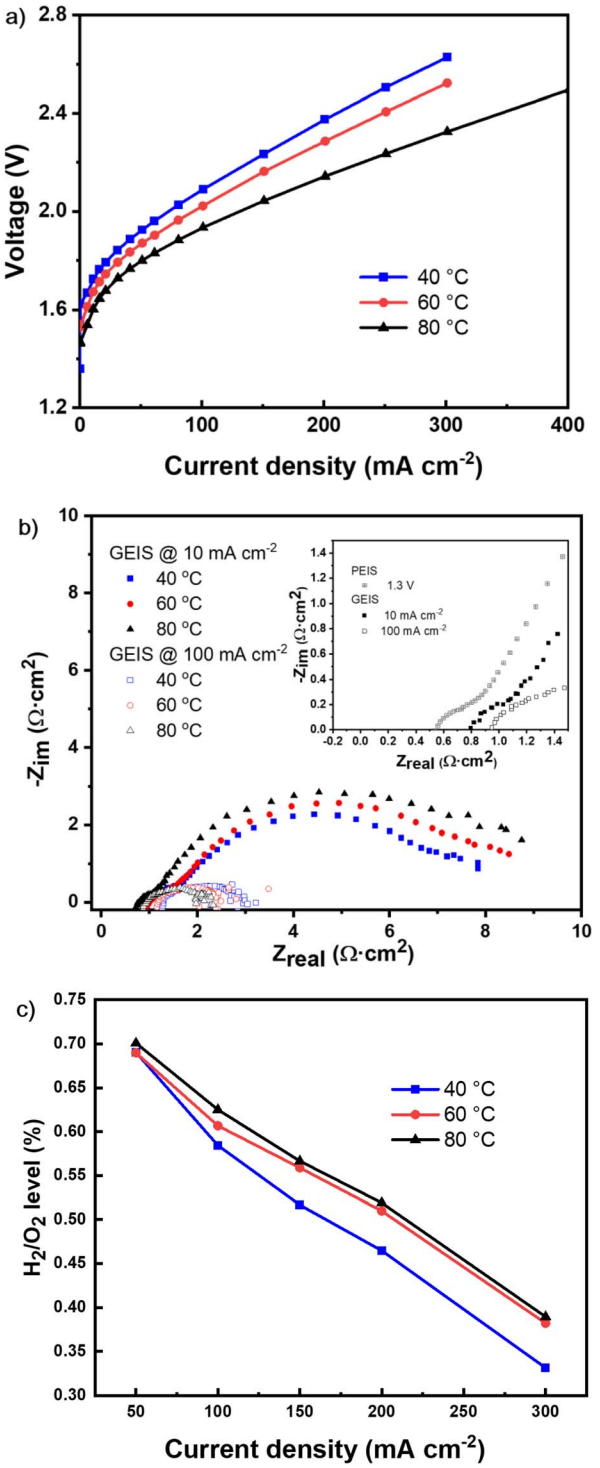

Fig. 6 (a) Water electrolysis polarization curves for cells assembled with P*m*DPipQ-50 membranes and nickel foam electrodes, and (b) the corresponding galvanostatic EIS data with an inset plot of the detailed potentiostatic and galvanostatic EIS data at 80 °C. (c) H_2 in O_2 concentrations reached at different current densities in AEMWEs assembled with P*m*DPipQ-50 at 40, 60, and 80 °C, respectively.

100 h between 40 and 80 °C, remained essentially constant. This further indicated the durability of P*m*DPipQ-50 in AEMWE applications.

4. Conclusions

A novel monomer *m*D, with two angled biphenyl units separated by an ethylene bridge, was synthesized to introduce polymer backbone flexibility in AEMs prepared by polyhydroxyalkylations. Copolymerization of *p*-terphenyl and *N*-methylpiperidone with controlled concentrations of *m*D, produced a series of AEMs with different ratios of flexible *m*D units and stiff *p*-terphenyl units. The *m*D monomer demonstrated high reactivity in the polyhydroxyalkylations and produced high-molecular weight polymers with varying backbone flexibility and good film-forming properties. Increasing contents of *m*D units promoted ionic clustering, as well as the uptake of water and electrolyte solution, which resulted in high ionic conductivities. Moreover, the presence of the *m*D units was found to improve both the thermal and alkaline stability of the AEMs. However, the *m*D content had seemingly limited impact on the alkaline stability, possibly because of small differences in the uptake of the alkaline solution and a limited effect of the *m*D units on the relaxation of the piperidinium rings along the polymer backbone. An AEMWE cell assembled with a selected AEM and plain nickel foam electrodes produced a current density of 402 mA cm^{-2} at 2.49 V. The results also indicated that further optimization of cell configuration and catalyst may significantly improve the performance of electrolyzers. The study demonstrated the high potential of introducing flexible chain segments to improve and tune AEMs for use in different electrochemical energy devices.

Author contributions

Si Chen: conceptualization, methodology, investigation, validation, writing – original draft. Yifan Xia: investigation, methodology, validation, writing – review & editing. David Aili: funding acquisition, supervision, writing – review & editing. Patric Jannasch: methodology, funding acquisition, supervision, writing – review & editing.

Conflicts of interest

There are no conflicts to declare.

Data availability

The materials and measurement methods used in this article have been included as part of the SI. See DOI: **https://doi.org/10.1039/d5ta04171f**.

Acknowledgements

We thank the Swedish Energy Agency (grants 50519-1, 45057-1, 37806-3, and 45515-3), the Swedish Research Council (grant 2023-04525), the Swedish Foundation for Strategic Research, SSF (grant ARC19-0026), and the European Union's Horizon 2020 Research and Innovation Action program (862509, NEXTAEC) for financial support. We also thank Dr Dmytro Serhiichuk for his assistance with the tensile testing.

References

1 U.S. Department of Energy, *Energy Earthshots Initiative*. **https://www.energy.gov/energy-earthshots-initiative**, accessed 2024-05-19.
2 M. Chatenet, B. G. Pollet, D. R. Dekel, F. Dionigi, J. Deseure, P. Millet, R. D. Braatz, M. Z. Bazant, M. Eikerling, I. Staffell, P. Balcombe, Y. S. Horn and H. Schafer, *Chem. Soc. Rev.*, 2022, **51**, 4583–4762.
3 J. Xue, J. Zhang, X. Liu, T. Huang, H. Jiang, Y. Yin, Y. Qin and M. D. Guiver, *Electrochem. Energy Rev.*, 2022, **5**, 348–400.
4 E. Park, P. Jannasch, K. Miyatake, C. Bae, K. Noonan, C. Fujimoto, S. Holdcroft, J. R. Varcoe, D. Henkensmeier, M. D. Guiver and Y. S. Kim, *Chem. Soc. Rev.*, 2024, **124**, 6393–6443.
5 D. Henkensmeier, W. C. Cho, P. Jannasch, J. Stojadinovic, Q. Li, D. Aili and J. O. Jensenm, *Chem. Rev.*, 2024, **53**, 5704–5780.
6 P. Zschocke and D. Quellmalz, *J. Membr. Sci.*, 1985, **22**, 325–332.
7 J. Yan and M. A. Hickner, *Macromolecules*, 2010, **43**, 2349–2356.
8 J. Yan, L. Zhu, B. L. Chaloux and M. A. Hickner, *Polym. Chem.*, 2017, **8**, 2442–2449.
9 H. Chen, R. Tao, K. T. Bang, M. Shao and Y. Kim, *Adv. Energy Mater.*, 2022, **12**, 2200934.
10 E. R. Peña, M. G. Zolotukhin and S. Fomine, *Macromolecules*, 2004, **37**, 6227–6235.
11 M. T. Guzmán-Gutiérrez, D. R. Nieto, S. Fomine, S. L. Morales, M. G. Zolotukhin, M. C. G. Hernandez, H. Kricheldorf and E. S. Wilks, *Macromolecules*, 2011, **44**, 194–202.
12 W. H. Lee, Y. S. Kim and C. Bae, *ACS Macro Lett.*, 2015, **4**, 814–818.
13 W. H. Lee, E. J. Park, H. Han, D. W. Shin, Y. S. Kim and C. Bae, *ACS Macro Lett.*, 2017, **6**, 566–570.
14 J. S. Olsson, T. H. Pham and P. Jannasch, *Adv. Funct. Mater.*, 2018, **28**, 1702758.
15 J. Wang, Y. Zhao and B. P. Setzler, *Nat. Energy*, 2019, **4**, 392–398.
16 D. Pan, P. M. Bakvand, T. H. Pham and P. Jannasch, *J. Mater. Chem. A*, 2022, **10**, 16478–16489.
17 D. Pan, S. Chen and P. Jannasch, *ACS Macro Lett.*, 2023, **12**, 20–25.
18 T. Jiang, C. Wu, Y. Zhou, S. Cheng, S. Yang, H. Wei, Y. Ding and Y. Wu, *J. Membr. Sci.*, 2022, **647**, 120342.
19 S. Chen, D. Pan, H. Gong and P. Jannasch, *Chem. Mater.*, 2024, **36**, 371–381.
20 B. Xue, W. Cui, S. Zhou, Q. Zhang, J. Zheng, S. Li and S. Zhang, *Macromolecules*, 2021, **54**, 2202–2212.
21 D. P. Leonard, S. Maurya, E. J. Park, L. D. Manriquez, S. Noh, X. Wang, C. Bae, E. D. Baca, C. Fujimoto and Y. S. Kim, *J. Mater. Chem. A*, 2020, **8**, 14135–14144.
22 W. Song, K. Peng, W. Xu, X. Liu, H. Zhang, X. Liang, B. Ye, H. Zhang, Z. Yang, L. Wu, X. Ge and T. Xu, *Nat. Comm.*, 2023, **14**, 2732.

23 T. H. Pham, J. S. Olsson and P. Jannasch, *J. Mater. Chem. A*, 2019, **7**, 15895–15906.
24 S. Zhang, W. Ma, L. Tian, D. Kong, Q. Zhu, F. Wang and H. Zhu, *ACS Appl. Mater. Inter.*, 2024, **16**, 7660–7669.
25 N. Chen, C. Hu, H. W. Wang, S. P. Kim, H. M. Kim, W. H. Lee, J. Y. Bae, J. H. Park and Y. M. Lee, *Angew. Chem., Int. Ed.*, 2021, **60**, 7710–7718.
26 C. Hu, J. H. Park, H. M. Kim, H. H. Wang, J. Y. Bae, N. Y. Kang, N. Chen and Y. M. Lee, *J. Membr. Sci.*, 2022, **647**, 120341.
27 L. W. Lai, H. Peng, Y. N. Ding, X. B. Yue, Q. G. Zhang, A. M. Zhu and Q. L. Liu, *J. Membr. Sci.*, 2024, **703**, 122837.
28 H. Lim, J. Y. Jeong, G. Shin, C. Kim, G. Choi, S. W. Myeong, S. M. Choi and T. Park, *Adv. Energy Mater.*, 2024, **14**, 2401725.
29 F. Xu, Y. Han, K. Huang, Y. Li, Q. Yang, J. Ding and B. Lin, *Chem. Mater.*, 2025, **37**, 2038–2046.
30 S. Chen and Y. C. Zhao, *Chin. J. Chem.*, 2020, **38**, 952–958.
31 J. Lv, S. Chen, Z. Xu, S. Zhang, Y. Li and Y. Zhao, *Macromolecules*, 2021, **54**, 3716–3724.
32 T. H. Pham, A. Allushi, J. S. Olsson and P. Jannasch, *Polym. Chem.*, 2020, **11**, 6953–6963.
33 A. Allushi, T. P. Pham, J. S. Olsson and P. Jannasch, *J. Mater. Chem. A*, 2019, **7**, 27164–27174.
34 P. Mansouri, D. Pan, A. Allushi and P. Jannasch, *Adv. Energy Mater.*, 2024, 2402869.
35 S. Chen and Y. C. Zhao, *Chin. J. Org. Chem.*, 2020, **40**, 3078–3093.
36 B. J. Fallon, V. Corcé, M. Amatore, C. Aubert, F. Chemla, F. Ferreira, A. Perez-Luna and M. Petit, *New J. Chem.*, 2016, **40**, 9912–9916.
37 M. Y. Gao and C. Gosmini, *Org. Lett.*, 2023, **25**, 7689–7693.
38 A. Allushi, P. M. Bakvand, H. Gong and P. Jannasch, *Mater. Adv.*, 2023, **4**, 3733–3745.
39 R. Gutru, Z. Turtayrva, F. Xu, G. Maranzana, B. Vigolo and A. Desforges, *Int. J. Hydrog. Energy*, 2020, **45**, 19642–19663.
40 D. Aili, M. R. Kraglund, S. C. Rajappan, S. Serhiichuk, Y. Xia, V. Deimede, J. Kallitsis, C. Bae, P. Jannasch, D. Henkensmeier and J. O. Jensen, *ACS Energy Lett.*, 2023, **8**, 1900–1910.
41 O. Bostrom, S. Choi, L. Xia, S. Meital, F. Lohmann-Richters and P. Jannasch, *J. Mater. Chem. A*, 2023, **11**, 21170–21182.
42 D. R. Dekel, S. Willdorf, U. Ash, M. Amar, S. Pusara, S. Dhara, S. Srebnik and C. E. Diesendruck, *J. Power Sources*, 2018, **375**, 351–360.
43 Y. Xia, S. C. Rajappan, D. Serhiichuk, M. R. Kraglund, J. O. Jensen and D. Aili, *J. Membr. Sci.*, 2023, **680**, 121719.
44 Y. Xia, S. C. Rajappan, S. Chen, M. R. Kraglund, D. Serhiichuk, D. Pan, J. O. Jensen, P. Jannasch and D. Aili, *ChemSusChem*, 2024, e202400844.
45 V. Schroder, B. Emonts, H. Janben and H. P. Schulze, *Chem. Eng. Technol*, 2004, **27**, 847–851.
46 P. Trinke, P. Haug, J. Brauns, B. Bensmann, H. Rauschenbach and T. Turek, *J. Electrochem. Soc.*, 2018, **165**, F502.
47 M. Trisno, A. Dayan, S. Lee, F. Egert, M. Gerle, M. Kraglund, J. Jensen, D. Aili, A. Roznowska, A. Michalak, H. Park, F. Razmjooei, S. Ansar and D. Henkensmeier, *Energy Environ. Sci.*, 2022, **15**, 4362–4375.
48 A. Dayan, D. Lee, K. Azizi, L. Cleemann, W. Cho and D. Henkensmeier, *Adv. Energy Mater.*, 2025, **15**, 2500498.